JOURNAL OF AIRCRAFT
Vol. 42, No. 1, January–February 2005

Application of Parameter Estimation to Improved Autogyro Simulation Model Fidelity

D. G. Thomson* and S. S. Houston†
University of Glasgow, Glasgow, Scotland G12 8QQ, United Kingdom

Development of an airworthiness design standard for light autogyros is underway in an attempt to improve a poor safety record. Mathematical modeling is playing a vital role in the understanding the flight mechanics of these rotorcraft. Unlike helicopters, autogyros have not received the attention of the technical community until recently, and, as a consequence, there is little theoretical analysis or experimental flight testing that makes use of contemporary methods. As a result, validity of mathematical modeling has relied on analysis of flight-test data from experiments conducted with two different aircraft. Parameter estimation by the use of a simple frequency-domain, equation-error approach has proved to yield consistent and robust results from each aircraft, highlighting the same mismatches between theory and experiment in both cases. In particular, primary damping derivatives for the heave and drag degrees of freedom, vital to ensure accurate modeling of short-period and phugoid mode damping, are shown to be substantially less than corresponding theoretical estimates. The flight estimates are used to guide parametric studies with the theoretical model in an attempt to understand and, hence, resolve discrepancies. Results suggest that propeller blockage effects and main rotor wake distortion could account for the gross discrepancies observed. It is concluded that the use of parameter estimation to compare theory and flight shows that autogyro characteristics are strongly influenced by these complex aerodynamic behaviors.

Nomenclature

A	=	system matrix
B	=	control matrix
M	=	perturbation in pitching moment
P, Q	=	roll and pitch rates
Q	=	rotor torque
q	=	perturbation in pitch rate
$\boldsymbol{u}$	=	control vector
u, w	=	perturbations in axial and heave velocities
V_f	=	flight speed
X, Z	=	perturbations in external forces
$\boldsymbol{x}$	=	state vector
$x_{\text{c.g.}}$, $y_{\text{c.g.}}$, z_c	=	position of center of gravity with respect to geometrical datum point of aircraft
x_{probe}, y_{probe}, z_{probe}	=	position of probe with respect to geometrical datum point of aircraft
α_{vane}	=	angle of attack at air data boom vane
β_{vane}	=	angle of sideslip at air data boom vane
θ	=	perturbation in pitch attitude
η_s	=	longitudinal shaft tilt
Ω	=	rotational speed of rotor

I. Introduction

THE development of the autogyro aircraft in the 1920s and 1930s paved the way for the development of the helicopter in the 1940s (Ref. 1). Many of the technical problems associated with rotary-wing flight had been discovered and rectified by early autogyro pioneers, most notably de la Cierva's solution of installing flap hinges to accommodate nonsymmetric lift from the rotor blades. The development of the autogyro receded as the helicopter became more popular and successful. In recent years, however, there has been a resurgence of interest in this type of aircraft, both as a recreational aircraft and as a low-cost alternative to the helicopter, with companies such as Groen and Cartercopter both seeking to market autogyro configurations to commercial and military operators.

The autogyro has become a very popular vehicle for hobby flying, possibly due to its flying characteristics, but also because they are often purchased in kit form, giving the owner the opportunity to the aircraft. This resurgence in interest in private flyers has also led to closer scrutiny by regulatory authorities. In particular, in the United Kingdom in the early 1990s, there were a series of fatal autogyro accidents in a very short time period, 6 in 2 years, from a very small fleet of around 100 aircraft. Investigation of these accidents was hindered by a lack of contemporary published research into this vehicle, particularly in its aerodynamic characteristics and its dynamics and flying qualities. This led the U.K. Civil Aviation Authority to fund research in these areas to support a major review of the British Civil Airworthiness Requirements (BCAR) for autogyros (BCAR Section T).[2] This, it is hoped, will improve the design standard of autogyros in the United Kingdom and improve their safety. This research involved wind-tunnel testing of an autgyro model, flight testing of two aircraft types, and development of comprehensive simulation models. Notable results include the first comprehensive study of the aerodynamics of an autogryo configuration,[3] but, more significantly, much more is now understood about the flight dynamic characteristics of this configuration.[4–7]

One of the main aims of the research was to modify an existing generic rotorcraft mathematical model, RASCAL[8] to simulate an autogyro, which could then be used to predict the stability of new or modified configurations. RASCAL is a nonlinear representation of a generic rotorcraft configuration as described in Sec. III of this paper. The flight tests carried out were in support of the modeling activity, the data recorded being used to validate the model as it was developed. The approach adopted was to linearize the RASCAL model representing the external forces and moments in the familiar stability derivatives form, as described in Sec. IV. Parameter estimation by the use of a simple frequency-domain, equation-error approach was then used to estimate the values of the stability derivatives from the recorded flight data, also in Sec. IV. Results from the first set of trials with a VPM aircraft (Fig. 1) were promising and gave good comparisons for many of the derivatives (Sec. V). However, there were significant errors in a number of places, including the damping derivatives for the drag and heave degrees of freedom. These derivatives are significant because they influence the damping of the phugoid and the short period modes. It is, therefore, essential

Received 18 July 2003; revision received 21 November 2003; accepted for publication 13 December 2003.

*Head of Department, Department of Aerospace Engineering.
†Senior Lecturer, Department of Aerospace Engineering.

Fig. 1 VPM M-16 G-BWGI.

Fig. 2 Montgomerie–Parsons flight research autogyro, University of Glasgow.

that improved predictions be obtained. A second series of trials in which the Department of Aerospace Engineering, University of Glasgow's Montgomerie autogyro were used (Fig. 2) gave results consistent with those from the VPM: good predictions in many areas, but inadequacies in the prediction of the damping derivatives for the drag and heave degrees of freedom.

In this paper, the process of identifying the reasons for these discrepancies and the approach used to resolve them is documented. Use is made of parameter estimation in a very practical and effective way to improve the predictions obtained significantly. This, in turn, will contribute to the revision of the BCAR Section T standards and flight safety.

II. Aircraft and Experimental Installations

Two aircraft were used in this study: the VPM M16 (Fig. 1) and the Montgomerie–Parsons (Fig. 2). These aircraft are produced in kit form for assembly by the owner. The former aircraft is of Italian origin with a maximum all-up mass of 450 kg. It is powered by a 90-kW piston engine driving a three-bladed fixed-pitch propeller. The latter is of U.K. design with a maximum all-up mass of 408 kg. It is powered by a 57-kW piston engine. In both cases, the engine drives a three-bladed fixed-pitch propeller. For helicopter engineers not familiar with autogyros, the rotor system is of an interesting configuration, typical of this class of aircraft. The two main rotor blades are bolted to a teeter bar, suspended from a teeter bolt. The blades are untwisted, and no cyclic pitch can be applied. This hub assembly is mounted on a spindle, about 200 mm long, and this spindle pivots about its lower end to tilt the entire rotor fore and aft and laterally to effect pitch and roll control, respectively.

The experimental installations used on both aircraft were broadly similar. Digital onboard recording systems recorded data at 10 Hz. Antialiasing filters were incorporated. A nose-mounted air data probe containing sideslip and angle-of-attack vanes was fitted, and an inertial unit measured angular velocities about three axes, as well as linear accelerations along these axes. A separate unit was used to measure roll and pitch angles. Pilot control positions were measured by the use of potentiometers. Rotorspeed was also recorded.

In the case of the VPM M16, the front seat and flight controls were removed to accommodate the system. It was found that the aircraft's own indicated airspeed system suffered from a position error of about 8 mph (3.6 m/s) across the speed range. All results for this aircraft are plotted with respect to the indicated airspeed, although the nose-mounted probe data were used for all analyses. The Montgomerie–Parsons aircraft was modified to accommodate the experimental system behind the pilot.

The identification of autogyro dynamics presents a particular challenge, in addition to those normally met with helicopter system identification. The aircraft is light, which demands stringent limits on atmospheric conditions during the tests. Solo operation of this aircraft was essential due to the mass and space restrictions imposed by the instrumentation system. This placed particular demands on the test pilot's flying skills, so that the quality of the test inputs were not compromised.

III. Description of Nonlinear Simulation Model RASCAL

It is appropriate to present brief details of the rotorcraft flight mechanics model, RASCAL, which is described more fully by Houston.[7,8] It is a generic rotorcraft simulation code, the nonlinear equations of motion taking the form

$$\dot{\boldsymbol{x}}\acute{Y} = f(\boldsymbol{x}, \boldsymbol{u}) \tag{1}$$

where the state vector $\boldsymbol{x}$ contains the airframe translational and angular velocity; blade flap, lag, and feather angles; rates for each blade on each rotor, the induced velocity states for each rotor wake, as well as the angular velocity of each rotor; and the engine torque. Elements of the control vector $\boldsymbol{u}$ are the four controls, which vary with aircraft type, for example, single main and tail rotor configurations will have three main rotor controls and one tail rotor control, and the autogyro will have fore/aft shaft tilt, lateral shaft tilt, rudder, and throttle. Blade attachment is modeled as offset hinges and springs, with a linear lag damper. The aerodynamic and inertial loads are represented by up to 20 elements per blade. Rotor blade element lift and drag forces are functions of section angle of attack and Mach number, derived from two-dimensional lookup tables. Airframe aerodynamic loads are functions of angle of attack and sideslip, also derived from two-dimensional lookup tables. Depending on the number of blades on each rotor, there can be up to 100 nonlinear, periodic ordinary differential equations describing the coupled rotor/airframe behavior. A simple model of the International Standard Atmosphere is used, with provision for variation in sea-level temperature and presssure.

The model is, therefore, a very conventional individual blade/blade element representation of a generic two-rotor aircraft. The rotor module is called twice in the simulation code, each rotor being discriminated by data that specify its location and orientation on the airframe and its characteristics in terms of blade mass distribution, hinge offset, and restraint, etc. In addition, a simple blockage factor, similar to that typically used for tail rotor applications,[9] can be specified when the rotor module is used to simulate the propeller of an autogyro.

IV. Data Analysis and Model Synthesis

The nonlinear representation given by Eq. (1) is linearized numerically to give the model structure for which coefficients are to be identified. This is of conventional state-space form, that is,

$$\dot{\boldsymbol{x}}\acute{Y} = A\boldsymbol{x} + B\boldsymbol{u} \tag{2}$$

where

$$A = \begin{bmatrix} X_u & X_w & X_q & X_\theta & X_\Omega \\ Z_u & Z_w & Z_q & Z_\theta & Z_\Omega \\ M_u & M_w & M_q & M_\theta & M_\Omega \\ 0 & 0 & 1 & 0 & 0 \\ Q_u & Q_w & Q_q & Q_\theta & Q_\Omega \end{bmatrix}, \qquad B = \begin{bmatrix} X_{\eta_s} \\ Z_{\eta_s} \\ M_{\eta_s} \\ 0 \\ Q_{\eta_s} \end{bmatrix} \tag{3}$$

$$\boldsymbol{x} = [u \quad w \quad q \quad \theta \quad \Omega]^T, \qquad \boldsymbol{u} = [\eta_s] \tag{4}$$

This constitutes the longitudinal subset of the conventional six-degree-of-freedom rigid- body flight mechanics model, with the important (and unique) addition of the rotorspeed degree of freedom. This is required due to the aircraft's operation in autorotation, the coupling of rotorspeed to the body modes being captured by the derivatives X_Ω, Z_Ω, and M_Ω. The rigid-body states are taken to be with respect to a mutually orthogonal, right-handed frame of reference whose origin is at the center of mass. The longitudinal and vertical axes are, respectively, parallel and normal to the keel of the aircraft. Trim and linearization are performed with the procedure described in Ref. 7. Reduction of the nonlinear model to the form given by equation (2) limits the bandwidth of applicability because rotor blade dynamics are treated in a quasi-steady manner by the linearization process.

The angular quantities in the state vector, and the control position, are all measured directly. The perturbations in translational velocities u and w are obtained from airspeed, sideslip, and angle of attack data measured at the nose-mounted boom, as follows:

$$U = U_{\text{probe}} - Q(z_{\text{vane}} - z_{\text{c.g.}}) + R(y_{\text{vane}} - y_{\text{c.g.}})$$
$$W = W_{\text{probe}} - P(y_{\text{vane}} - y_{\text{c.g.}}) + Q(x_{\text{vane}} - x_{\text{c.g.}}) \tag{5}$$

where

$$U_{\text{probe}} = \frac{V_f \cos\beta_{\text{vane}}}{\sqrt{1 + \tan^2\alpha_{\text{vane}}}}, \qquad W_{\text{probe}} = U_{\text{probe}} \tan\alpha_{\text{probe}} \tag{6}$$

Of course, if U_e is the equilibrium or trim value of U at the relevant flight condition, then

$$U = U_e + u$$

etc.

The time histories of each variable were then converted into frequency domain information using a discrete Fourier transform (see Ref. 10) given by

$$X(k\Delta f) = \Delta t \sum_{n=0}^{N-1} x_n \exp\left[\frac{-i2\pi(kn)}{N}\right]$$
$$k = 0, 1, 2, \ldots, N-1 \tag{7}$$

which gives real and imaginary parts of X,

$$\text{Re}[X(k\Delta f)] = \Delta t \sum_{n=0}^{N-1} x_n \cos\left[\frac{2\pi(kn)}{N}\right]$$
$$\text{Im}[X(k\Delta f)] = -\Delta t \sum_{n=0}^{N-1} x_n \sin\left[\frac{2\pi(kn)}{N}\right] \tag{8}$$

The quality of these frequency domain data can be enhanced by standard processing techniques such as applying overlapped and tapered windows to the data, as recommended by Tischler.[10]

Each degree of freedom can then be treated separately, and formulation as a linear regression problem allows estimation of the coefficients. The state-space description is converted to the frequency domain, that is,

$$i\omega\boldsymbol{x}\ (\omega) = A\boldsymbol{x}(\omega) + B\boldsymbol{u}(\omega) \tag{9}$$

Note that this assumes that any process noise is zero. The unknown coefficients of the A and B matrices are determined by solutions of the frequency-domain equations

$$-\omega\text{Im}[\boldsymbol{x}(\omega)] = A\{\text{Re}[\boldsymbol{x}(\omega)]\} + B\{\text{Re}[\boldsymbol{u}(\omega)]\}$$
$$\omega\text{Re}[\boldsymbol{x}(\omega)] = A\{\text{Im}[\boldsymbol{x}(\omega)]\} + B\{\text{Im}[\boldsymbol{u}(\omega)]\} \tag{10}$$

This solution applies equal weighting to real and imaginary part errors, which is consistent with the standard weighting for system identification on a Bode plot. The pitching moment equation, for example, is then expressed as the two equations

$$-\omega\text{Im}[q(\omega)] = M_u\text{Re}[u(\omega)] + M_w\text{Re}[w(\omega)] + M_q\text{Re}[q(\omega)]$$
$$+ M_\theta\text{Re}[\theta(\omega)] + M_\Omega\text{Re}[\Omega(\omega)] + M_{\eta_s}\text{Re}[\eta_s(\omega)]$$
$$\omega\text{Re}[q(\omega)] = M_u\text{Im}[u(\omega)] + M_w\text{Im}[w(\omega)] + M_q\text{Im}[q(\omega)]$$
$$+ M_\theta\text{Im}[\theta(\omega)] + M_\Omega\text{Im}[\Omega(\omega)] + M_{\eta_s}\text{Im}[\eta_s(\omega)] \tag{11}$$

None of the parameter variables in the model structure (3) are fixed during the estimation process. This approach is not new,[11–14] but, in application, it serves to illustrate that a simple method can be used to obtain robust identification of autogyro longitudinal stability and control derivatives using relatively straightforward frequency-domain parameter estimation tools.

V. Modeling Requirements for Demonstration of Compliance with BCAR Section T

The level of sophistication afforded by RASCAL is necessary because it is essential to be able to predict the dynamic properties of the aircraft adequately over the full six-degree-of-freedom bandwidth. This is best illustrated by consideration of the BCAR Section T requirements. The dynamic stability criteria of these requirements relate acceptable levels of damping to period of oscillation, T:

1) If $T < 5$ s, damp to one-half amplitude in not more than one cycle.

2) If $5 < T < 10$, damp to one-half amplitude in not more than two cycles.

3) If $10 < T < 20$, oscillation must be damped.

4) If $T > 20$, time to double amplitude must be greater than 20 s if unstable.

These criteria can be presented as shown in Fig. 3, any oscillatory mode placed to the right of the compliance boundary being acceptable. To use simulation to demonstrate compliance with BCAR Section T, the mathematical model must predict those stability derivatives that influence damping or frequency accurately.

The longitudinal dynamic characteristics of autogyros more closely resemble those of a conventional aircraft than a helicopter, that is, it is normal to observe a short period mode associated with the pitch axis degree of freedom and a longer period phugoid motion associated with oscillations in airspeed and altitude. The damping

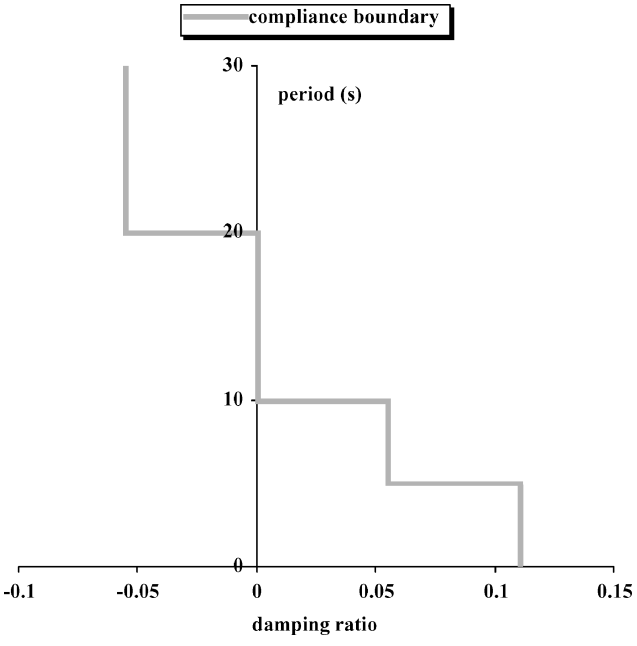

Fig. 3 BCAR Section T, dynamic stability compliance criteria.

of the phugoid is strongly influenced by the drag damping derivative X_u, whereas the heave damping derivative Z_w has a significant impact on the short period damping for the autogyro types examined here. It follows that there is a need to ensure reliable prediction of these two derivatives. Furthermore, as might be expected of an aircraft operating in autorotation, accurate prediction of the rotor speed is essential. Associated with this is the need for good prediction of the rotor torque derivative with respect to rotor speed Q_Ω. In piloting terms, control of rotor speed is a major factor in flying autogyros. Sudden loss of rotor speed in maneuvering flight has been attributed as the cause of many accidents, and, hence, this derivative is significant in the determination of flying qualities.

VI. Initial Comparison of Results from VPM M16 and Montgomerie–Parsons Flight Tests

Frequency sweep inputs were used to excite the aircraft over a broad frequency range. The VPM M16 aircraft characteristics are such that the longitudinal stick input conventionally begins at low frequency (Fig. 4), with an upper frequency limit of 4 Hz. The Montgomerie–Parsons aircraft, however, is marginally stable, and a modified technique was attempted, starting at high frequency and then reducing until the unstable mode was excited (Fig. 5). An important aspect of any identification study is the identifiability of the estimated parameters. This is particularly germane to the equation error approach. Robust estimates of the derivatives are those whose values can be judged to be invariant with the event, input type, estimation method, or frequency range used, and for which a low standard error is calculated. The issue of identifiability is particularly germane to the autogyro problem because there is little literature on the vehicle's characteristics. Houston[5] deals comprehensively with such identifiability issues for the VPM M16 aircraft.

Figure 6 shows a comparison of values of X_u and Z_w as estimated from flight-test results (with the approach detailed in Sec. IV) and those from the simulation model RASCAL. These data comes from the first set of flight trials using the VPM M16 aircraft (Fig. 1). It is clear from Fig. 6 that the predictions of these derivatives is poor across the aircraft's speed range. Note that the flight-test results are presented as 95% confidence bounds. Figure 7 shows the corresponding results for the Montgomerie–Parsons aircraft, which exhibit a similar trend: The mathematical model underpredicts the value of both derivatives across the speed range. There is, therefore, a consistency in the results that indicates deficiencies in the model in

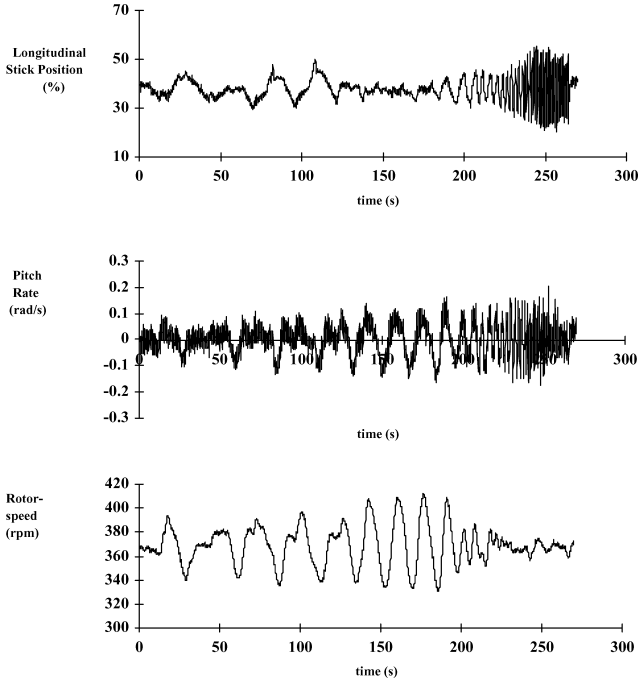

Fig. 4 VPM M16 response during frequency sweep test at 70 mph.

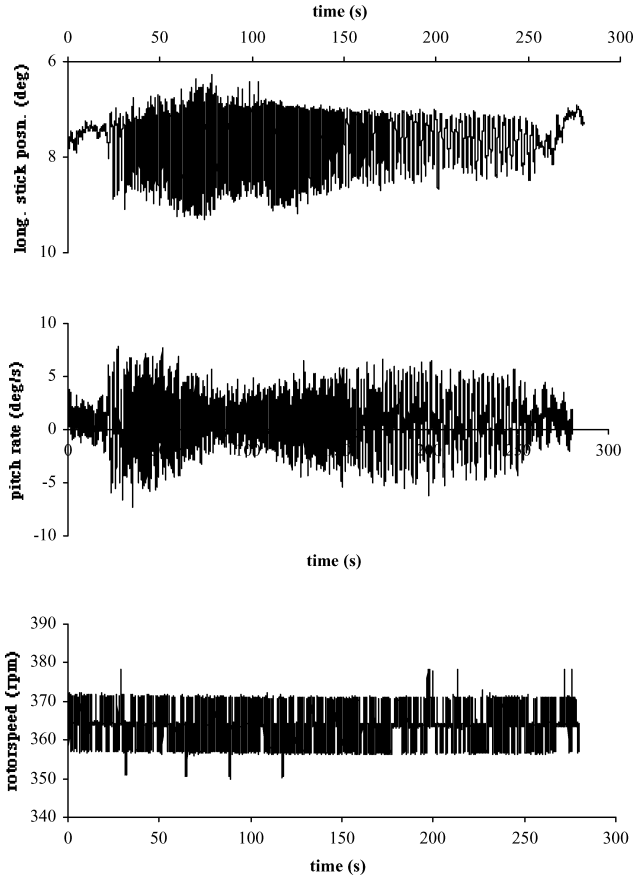

Fig. 5 Montgomerie–Parsons response during frequency sweep, 60 mph.

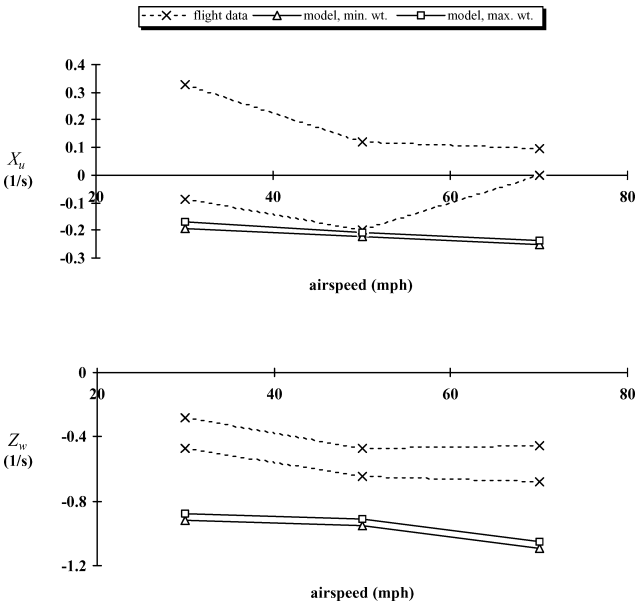

Fig. 6 Flight and simulation comparisons of drag and heave damping derivatives (VPM M16).

predicting these derivatives. These deficiencies must be addressed to ensure adequate predictive capabilities.

Good prediction of rotor speed is essential for any rotorcraft simulation, but this is particularly true in the autorotative flight of the autogyro. A comparison of predicted rotor speed as a function of trim flight speed for the VPM M16 is presented in Fig. 8a and the associated rotor torque derivative in Fig. 8b. Note that the model consistently underpredicts rotor speed by around 25 rpm across the

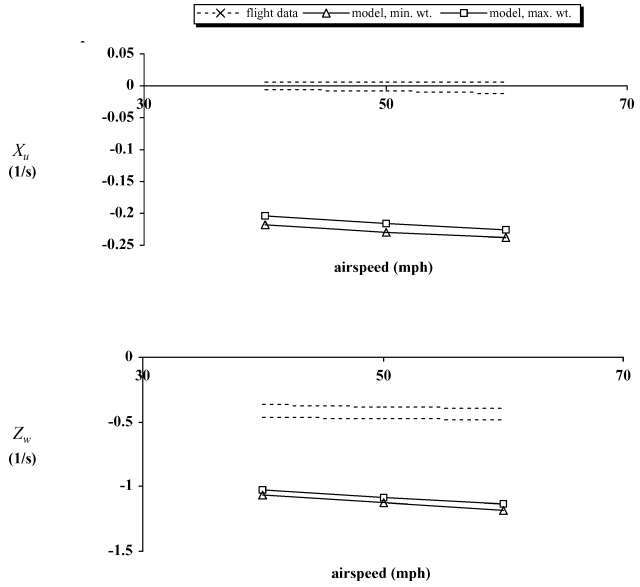

Fig. 7 Flight and simulation comparisons of drag and heave damping derivatives (Montgomerie–Parsons).

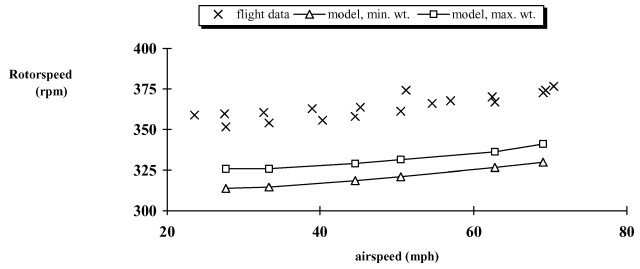

Fig. 8a Flight and simulation comparison of rotorspeed for VPM M16.

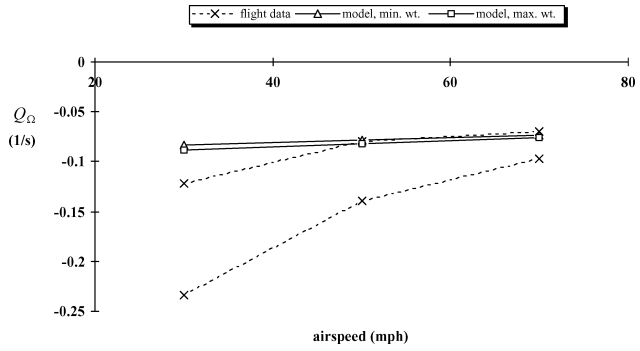

Fig. 8b Flight and simulation comparison of rotor torque damping, VPM M16.

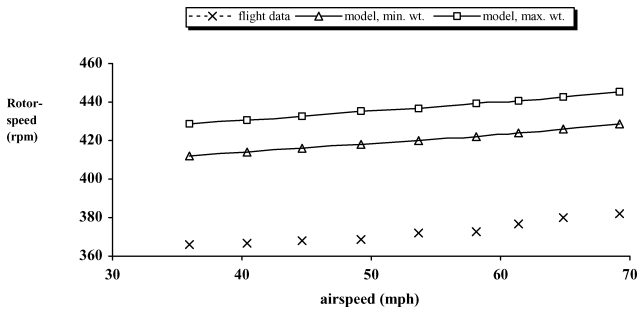

Fig. 9a Flight and simulation comparison of rotorspeed for Montgomerie–Parsons.

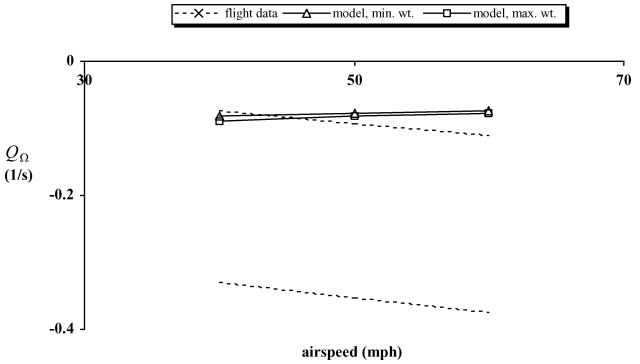

Fig. 9b Flight and simulation comparison of rotortorque damping, Montgomerie–Parsons.

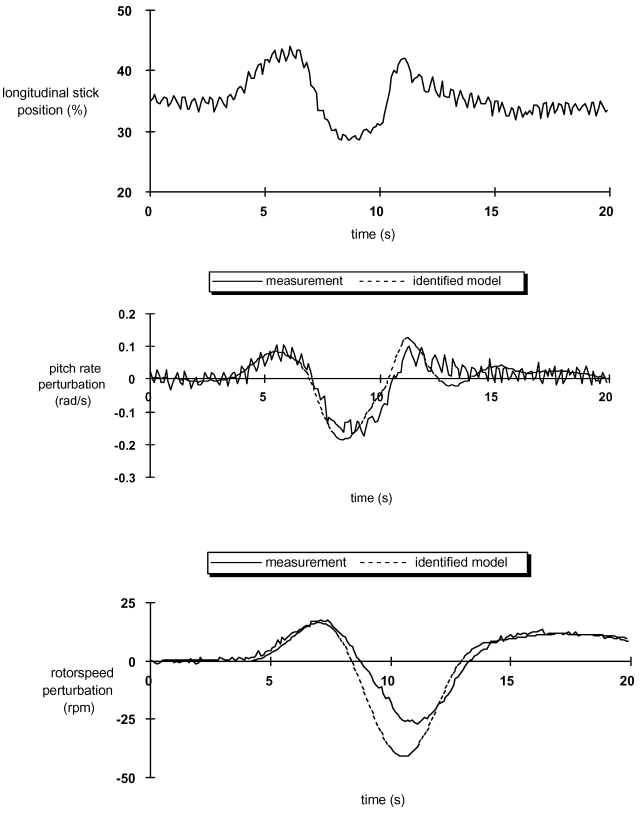

Fig. 10 VPM M16 identified model verification, 70 mph, short-term response.

speed range for the VPM. The rotor torque derivative is predicted well (Fig. 8b), either lying inside the bounds or close to them across the speed range. These results are, however, acceptable in the context of contemporary rotorcraft simulations. Figure 9a shows the comparison of predicted rotor speed against measured rotor speed for the Montgomerie–Parsons aircraft, whereas Fig. 9b compares the rotor torque derivative. The rotor speed comparison shows a consistent 60 rpm overprediction across the speed range, whereas at best, the rotor torque derivative falls within the error bounds at low speed only. The better rotor speed prediction for the VPM aircraft is most likely because much better data were available for the blade section used in this aircraft. In fact, a full cpmputational fluid dynamics computation was performed to back up the available wind-tunnel data.

The fidelity of these flight-identified models is established by comparison of their predictive ability by the use of response data from a test input dissimilar to that used in the identification process.[5] A typical result is shown in Fig. 10 for the VPM M16 aircraft. The fidelity of the theoretical model is established by comparison of the

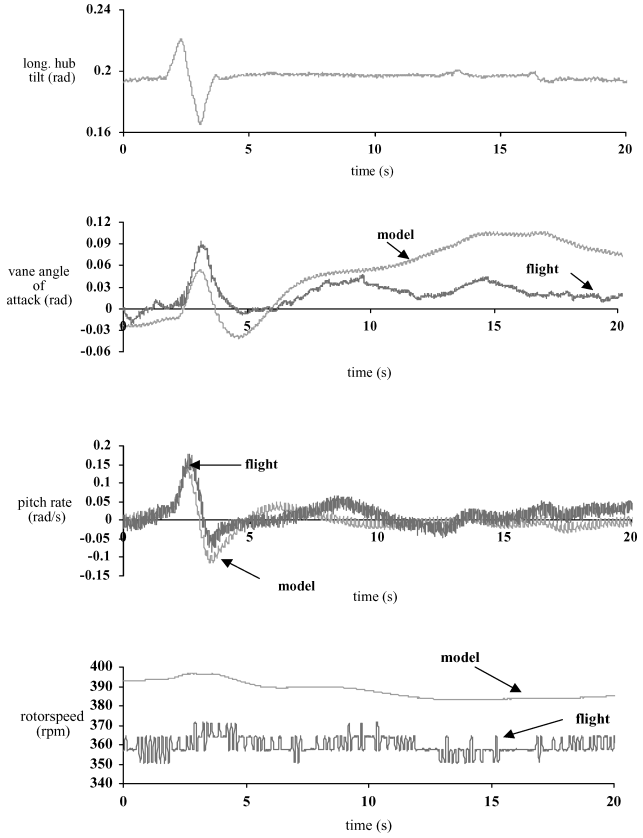

Fig. 11 Nonlinear model comparison with flight test (doublet input, 50 mph).

response to a control input measured in flight with that of the model when driven by the same input. Figure 11 shows a typical result for the Montgomerie–Parsons aircraft.

In summary, the model predictions for both aircraft are consistently poor for both X_u and Z_w; however, the predictions of rotor speed and rotor torque derivative Q_Ω are significantly better for the VPM than the Montgomerie–Parsons.

VII. Empirical Correction of Model Using Parameter Estimation

Although the RASCAL simulation model provides a high level of fidelity for many helicopter applications, it is clear from the foregoing sections that there are deficiencies in simulating autogyros. These are discussed individually hereafter, and in each case the flight results originating from parameter estimation are used to obtain an empirical correction to the model to improve its fidelity. This applied process is a pure tuning procedure. However, because the theoretical model deficiencies are common to both aircraft types, the results tend to suggest that the tuning parameters and their numerical values constitute parametric model extensions and are, therefore, transferable to other similar configurations.

A. Speed and Heave Damping Derivatives, X_u and Z_w

Perhaps the most obvious area that might be suspected when the poor prediction of drag damping is considered is the aerodynamic representation of the vehicle airframe. In the case of the VPM, the simulation uses wind-tunnel data of a representative model[3] and so there is a high level of confidence that this is not the source of error. The rotor, with its large inertia, is also likely to be insensitive to disturbances in forward speed, and so attention is focussed on the only other significant component of the aircraft, namely, the propeller. This assessment is verified by the data presented in Table 1, which details the breakdown of contributions to the derivative X_u by the propeller, airframe, and rotor, the propeller contribution being by far the most significant.

Table 1 Breakdown of drag damping derivative, Montgomerie–Parsons

Airspeed, mph (m/s)	Propeller	Airframe	Rotor	Total
40 (18)	−0.111	−0.035	−0.07	−0.216
50 (22)	−0.143	−0.04	−0.063	−0.246
60 (27)	−0.15	−0.05	−0.06	−0.260

Table 2 Breakdown of heave damping derivative, Montgomerie–Parsons

Airspeed (mph)	Propeller	Airframe	Rotor	Total
40	−0.0685	−0.1175	−0.9225	−1.0850
50	−0.0675	−0.1365	−0.9725	−1.1765
60	−0.0675	−0.1615	−1.0195	−1.2485

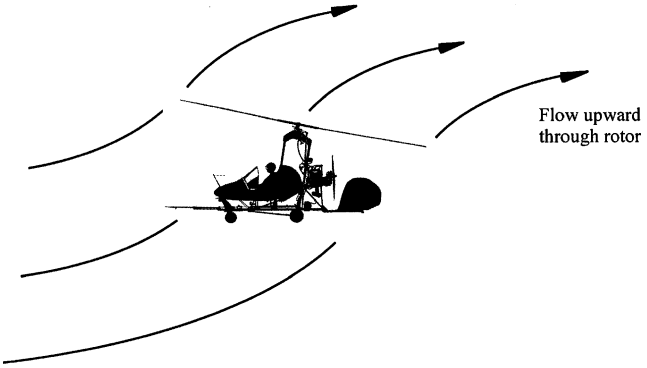

Fig. 12 Schematic of postulated inflow distortion in autorotative flight.

Both aircraft are characterized by pusher propellers located behind the pod. There is, therefore, a large degree of blockage due to the pilot, pod, and engine masking the propeller. It is a relatively simple process to include a blockage factor in the propeller model, and this can be tuned by the use of parameter-estimation-derived flight results to compare the value of X_u with that estimated from flight. When a similar check is performed on the heave damping derivative Z_w (Table 2), it is clear that the major contribution comes from the rotor. Again, this is predictable because disturbances in heave velocity w, that is, angle of attack, are likely to have little effect on the propeller forces and only a limited effect on airframe aerodynamic forces, which are small anyway. Conversely, even small changes of angle of attack at the rotor disk can make large changes to the magnitude and direction of the thrust generated. Figure 12 shows schematically the expected flow direction up through the autogyro rotor. There are complex interactional aerodynamic features caused by both the flow around the airframe and the close proximity of the propeller with the rotor before the air reaches the underside of the disk. This, of course, is different from the helicopter, where air is accelerated from a clean region of air above the rotor down over the fuselage. These interactional aerodynamics are difficult to model; however, it is postulated here that their effect will be somewhat akin to dihedral on a high-winged aircraft, that is, a local change in angle of attack.

Figure 13 shows the effect of these modeling enhancements on the results for the VPM M16. Two changes have been made to the model. First, it is assumed that the presence of the airframe results in total blockage of the propeller to the oncoming airstream. The second modification replaces the conventional kinematic calculation of angle of attack at the rotor hub by an assumption that the angle of attack here will be one-half of the angle of attack at the center of gravity. This is simply to take into account the skewing of the wake as it approaches the rotor disc due to aerodynamic interaction. Figure 13 shows that X_u and Z_w are brought inside the confidence bounds over most of the speed range.

In the context of demonstrating compliance with BCAR section T, the migration of the phugoid mode with flight speed is plotted for

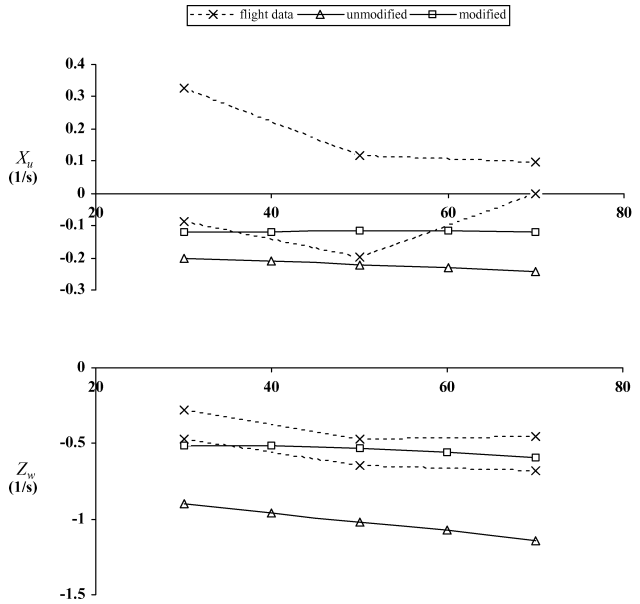

Fig. 13 Flight and modified simulation comparisons of drag and heave damping derivatives (VPM M16).

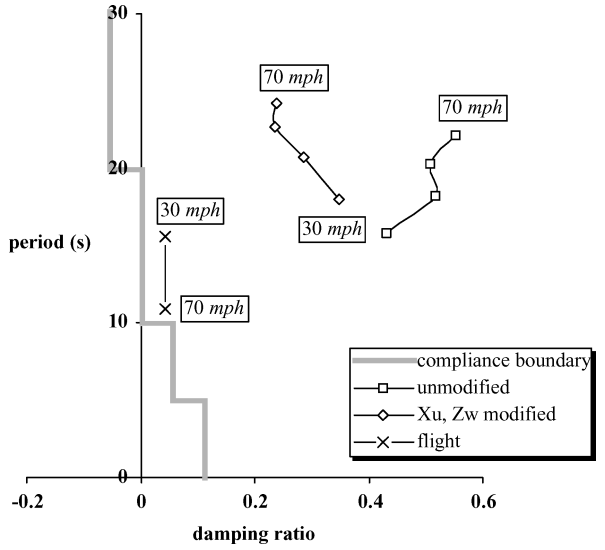

Fig. 14 Model and flight comparisons of VPM M16 compliance with BCAR Section T.

the flight data and the modified and unmodified simulation results in Fig. 14, the unmodified results being plotted at 10-mph increments. The flight data show a lightly damped oscillation with period varying between 12 and 15 s. Because this lies to the right of the compliance boundary, this is an acceptable characteristic; however, its proximity to the boundary indicates that this is only marginally acceptable. The unmodified simulation predicts too much damping, but with the addition of the two modifications described earlier, the predicted mode is pulled toward the flight-measured values.

B. Rotor Speed and Torque Derivative

Blade section drag characteristics have a major impact on trim rotorspeed, which, for the Montgomerie–Parsons aircraft, is poorly predicted. However, the rotor torque derivative Q_Ω is, to first order, proportional to the section drag coefficient, and comparison of flight estimates with theory can, therefore, be used to tune the model. The blade section is a NACA 8H12, data for which are available for a range of Reynolds numbers and skin characteristics.[15] The results shown in Figs. 7a and 7b are consistent and show that a low value of blade drag coefficient is being used. Figure 15b shows that the

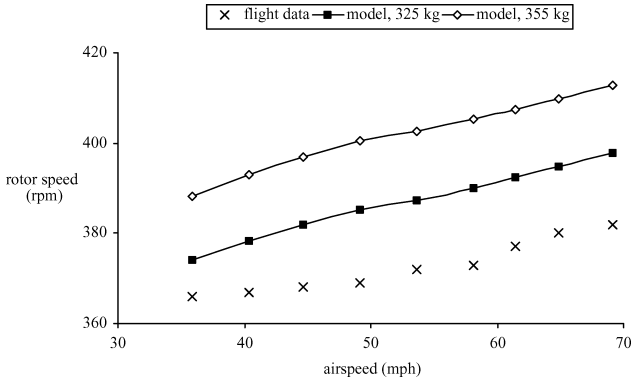

Fig. 15a Flight and modified simulation comparison of rotorspeed, Montgomerie–Parsons.

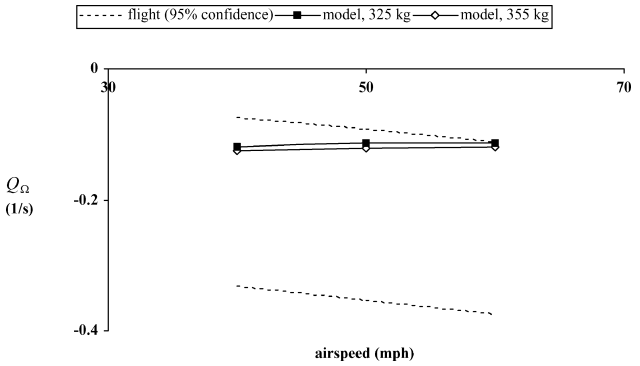

Fig. 15b Flight and modified simulation comparison of rotor torque damping, Montgomerie–Parsons.

magnitude of Q_Ω is increased by an increase of the blade profile drag to the values given in Ref. 15 for maximum roughness. This places Q_Ω just within the flight bounds (Fig. 7b), and Fig. 15a shows the effect on rotor speed. The 60-rpm rotor speed overprediction (Fig. 7a), is reduced to an overprediction of just 15 rpm (Fig. 15a).

VIII. Conclusions

The work documented in this paper demonstrates the use of parameter estimation to identify and remedy deficiencies in a rotorcraft mathematical model when applied to the autogyro configuration. Very specific problems relating to the rotor speed degree of freedom, drag damping, and heave damping were identified. The cause of the deficiencies in the rotor degree of freedom was identified as poor blade section aerodynamics modeling: A situation that is relatively simple to rectify with improved data. However, one of the major conclusions of this work is that interactional aerodynamics between the rotor, propeller, and the airframe are extremely influential in autogyros, and this must be taken into account in the construction of mathematical models. A more general conclusion is that parameter estimation has been used here in a very practical and effective way to enhance that mathematical model that will be used to improve the safety of a whole class of aircraft.

References

[1]Leishman, J. G., "The Development of the Autogiro: A Technical Perspective," *From Autogiro to Gyroplane—The Past, Present and Future of an Aviation History*, Hofstra Univ., NY, April 2003.

[2]Anon., "British Civil Airworthiness Requirements, Section T, Light Gyroplane Design Requirements," Civil Aviation Authority Paper No. T 860, Issue 2, July 1993.

[3]Coton, F., Smrcek, L., and Patek, Z., "Aerodynamic Characteristics of a Gyroplane Configuration," *Journal of Aircraft*, Vol. 35, No. 2, 1998, pp. 274–279.

[4]Houston, S. S., "Longitudinal Stability of Gyroplanes," *Aeronautical Journal*, Vol. 100, No. 991, 1996, pp. 1–6.

[5]Houston, S. S., "Identification of Autogyro Longitudinal Stability and Control Characteristics," *Journal of Guidance, Control, and Dynamics*, Vol. 21, No. 3, 1998, pp. 391–399.

[6]Houston, S. S., "Identification of Gyroplane Lateral/Directional Stability and Control Characteristics From Flight Test," *Proceedings of the Institute of Mechanical Engineers*, Vol. 212, Pt. G, 1998, pp. 271–285.

[7]Houston, S. S., "Validation of a Rotorcraft Mathematical Model for Autogyro Simulation," *Journal of Aircraft*, Vol. 37, No. 3, 2000, pp. 403–409.

[8]Houston, S. S., "Validation of a Non-linear Individual Blade Rotorcraft Flight Dynamics Model Using a Perturbation Method," *Aeronautical Journal*, Vol. 98, No. 977, 1994, pp. 260–266.

[9]Prouty, R., *Helicopter Performance, Stability, and Control*, Krieger, Malabar, FL, 1990, pp. 285–287.

[10]Tischler, M. B., *Identification Techniques, Frequency Domain Methods*, LS178, AGARD, Oct. 1991, pp. 6-1 to 6-4.

[11]Feik, R. E., and Perrin, R. H., "Identification of an Adequate Model for Collective Response Dynamics of a Sea King Helicopter in Hover," *Vertica*, Vol. 13, No. 3, 1989, pp. 251–265.

[12]Duval, R., Bruhic, O., and Green, J., "Identification of a Coupled Flapping/Inflow Model for the Puma Helicopter from Flight Test Data," *Vertica*, Vol. 13, No. 3, 1989, pp. 267–274.

[13]Tischler, M. B., Leung, J. G. M., and Dugan, D. C., "Frequency-Domain Identification of XV-15 Tiltrotor Aircraft Dynamics in Forward Flight," *Journal of the American Helicopter Society*, Vol. 30, No. 2, 1985, pp. 38–48.

[14]Tischler, M. B., Fletcher, J. W., Drikmann, V. L., Williams, R. A., and Cason, R. W., "Demonstration of Frequency-Sweep Testing Technique Usng a Bell 214-ST Helicopter," NASA TM 89422, 1987.

[15]Schaefer, R. F., and Smith, H. A., "Aerodynamic Characteristics of the NACA 8-H-12 Airfoil Section at Six Reynolds Numbers," NACA TN 1998, Dec. 1948.